J|A|C|S
ARTICLES
Published on Web 06/02/2007

# Monomeric and Heterodimeric Triple Helical DNA Mimics

Ivan Trkulja and Robert Häner*

*Contribution from the Department of Chemistry and Biochemistry, University of Bern, Freiestrasse 3, CH-3012 Bern, Switzerland*

Received March 5, 2007; E-mail: robert.haener@ioc.unibe.ch

***Abstract:*** The construction of artificial triple helical structures with oligonucleotides containing non-nucleosidic phenanthrenes and pyrenes is described. The polyaromatic building blocks, which are used as connectors between the *Hoogsteen* strand and the Watson-Crick hairpin, lead to a significant stabilization of intramolecular triple helices. Description of the relative orientation of pyrene building blocks is rendered possible by the observation of exciton coupling in the *circular dichroism* spectra. In addition, the formation of heterodimeric triple helical constructs is explored. Again, the polyaromatic residues are found to have a positive effect on the stability of these structures. The results are important for the design and construction of nucleic-acid-based, triple helical architectures. Furthermore, they will help in the development of analogues of biologically important, naturally occurring triplex structures.

## Introduction

Triple helical DNA structures have been a subject of vast research in the past 50 years.[1−6] Triple helix formation is generally limited to homopurine/homopyrimidine regions of a DNA duplex. Binding of the third strand involves formation of Hoogsteen (*parallel* or *pyrimidine motif*) or reverse-Hoogsteen bonds (*antiparallel* or *purine motif*) to the purine strand in the major groove. Since triple helix formation takes place in a highly specific manner it has found wide interest as a method of selectively targeting DNA[7−11] for gene-based diagnostic and pharmaceutical applications. Double stranded DNA containing homopurine/homopyrimidine stretches was also shown to disproportionate into a triple and a single stranded region (H-DNA) under certain conditions, such as physical constraints and low pH.[12−14] Furthermore, synthetic oligonucleotides were shown to adopt intramolecular triple helical structures[15−24] or *clamp-type* motifs.[25−29] In view of the abundance of different types of triplex structures observed in vitro, the question regarding the occurrence and potential biological significance of triple helical structures of nucleic acids in vivo has been intensively investigated and reviewed.[14] In particular, *potential intrastrand triplex elements* were identified and investigated in the genome of *Escherichia coli*.[30,31] In light of the biological importance of such sequences, we became interested in the synthesis and investigation of structural mimics of intramolecular triple helices. Such mimics may serve as chemically and structurally stable analogues of naturally occurring structures.[19,22,32−36] In our work aimed at the development of DNA mimics, we reported the synthesis of non-nucleosidic, polyaro-

(1) Felsenfeld, G.; Davies, D. R.; Rich, A. *J. Am. Chem. Soc.* **1957**, *79*, 2023−2024.
(2) Le Doan, T.; Perrouault, L.; Praseuth, D.; Habhoub, N.; Decout, J. L.; Thuong, N. T.; Lhomme, J.; Hélène, C. *Nucleic Acids Res.* **1987**, *15*, 7749−7760.
(3) Moser, H. E.; Dervan, P. B. *Science* **1987**, *238*, 645−650.
(4) Francois, J. C.; Saison-Behmoaras, T.; Hélène, C. *Nucleic Acids Res.* **1988**, *16*, 11431−11440.
(5) Frank-Kamenetskii, M. D.; Mirkin, C. M. *Annu. Rev. Biochem.* **1995**, *64*, 65−95.
(6) Roberts, R. W.; Crothers, D. M. *Science* **1992**, *258*, 1463−1466.
(7) Hélène, C.; Toulmé, J. J. *Biochim. Biophys. Acta* **1990**, *1049*, 99−125.
(8) Maher, L. J., III. *Bioessays* **1992**, *14*, 807−815.
(9) Maher, L. J., III. *Cancer Invest.* **1996**, *14*, 66−82.
(10) Fox, K. R. *Curr. Med. Chem.* **2000**, *7*, 17−37.
(11) Buchini, S.; Leumann, C. J. *Curr. Opin. Chem. Biol.* **2003**, *7*, 717−726.
(12) Mirkin, S. M.; Lyamichev, V. I.; Drushlyak, K. N.; Dobrynin, V. N.; Filippov, S. A.; Frank-Kamenetskii, M. D. *Nature* **1987**, *330*, 495−497.
(13) Mirkin, S. M.; Frank-Kamenetskii, M. D. *Annu. Rev. Biophys. Biomol. Struct.* **1994**, *23*, 541−576.
(14) Zain, R.; Sun, J. S. *Cell. Mol. Life Sci.* **2003**, *60*, 862−870.
(15) Sklenar, V.; Feigon, J. *Nature* **1990**, *345*, 836−838.
(16) Häner, R.; Dervan, P. B. *Biochemistry* **1990**, *29*, 9761−9765.
(17) Pilch, D. S.; Brousseau, R.; Shafer, R. H. *Nucleic Acids Res.* **1990**, *18*, 5743−5750.
(18) Chen, F. M. *Biochemistry* **1991**, *30*, 4472−4479.
(19) Durand, M.; Peloille, S.; Thuong, N. T.; Maurizot, J. C. *Biochemistry* **1992**, *31*, 9197−9204.
(20) Völker, J.; Botes, D. P.; Lindsey, G. G.; Klump, H. H. *J. Mol. Biol.* **1993**, *230*, 1278−1290.
(21) Radhakrishnan, I.; Patel, D. J. *Structure* **1993**, *1*, 135−152.
(22) Bartley, J. P.; Brown, T.; Lane, A. N. *Biochemistry* **1997**, *36*, 14502−14511.
(23) Gondeau, C.; Maurizot, J. C.; Durand, M. *Nucleic Acids Res.* **1998**, *26*, 4996−5003.
(24) Hoyne, P. R.; Gacy, A. M.; McMurray, C. T.; Maher, L. J., III. *Nucleic Acids Res.* **2000**, *28*, 770−775.
(25) Xodo, L. E.; Manzini, G.; Quadrifoglio, F. *Nucleic Acids Res.* **1990**, *18*, 3557−3564.
(26) Giovannangeli, C.; Thuong, N. T.; Hélène, C. *Proc. Natl. Acad. Sci. U.S.A.* **1993**, *90*, 10013−10017.
(27) Kandimalla, E. R.; Agrawal, S. *Biochemistry* **1996**, *35*, 15332−15339.
(28) Ryan, K.; Kool, E. T. *Chem. Biol.* **1998**, *5*, 59−67.
(29) Maksimenko, A. V.; Volkov, E. M.; Bertrand, J. R.; Porumb, H.; Malvy, C.; Shabarova, Z. A.; Gottikh, M. B. *Eur. J. Biochem.* **2000**, *267*, 3592−3603.
(30) Hoyne, P. R.; Edwards, L. M.; Viari, A.; Maher, L. J., III. *J. Mol. Biol.* **2000**, *302*, 797−809.
(31) Hoyne, P. R.; Maher, L. J. *J. Mol. Biol.* **2002**, *318*, 373−386.
(32) Tarkoy, M.; Phipps, A. K.; Schultze, P.; Feigon, J. *Biochemistry* **1998**, *37*, 5810−5819.
(33) Salunkhe, M.; Wu, T.; Letsinger, R. L. *J. Am. Chem. Soc.* **1992**, *114*, 8768−8772.
(34) Bevers, S.; Schutte, S.; McLaughlin, L. W. *J. Am. Chem. Soc.* **2000**, *122*, 5905−5915.
(35) Stutz, A.; Langenegger, S. M.; Häner, R. *Helv. Chim. Acta* **2003**, *86*, 3156−3163.
(36) Li, H.; Broughton-Head, V. J.; Peng, G. M.; Powers, V. E. C.; Ovens, M. J.; Fox, K. R.; Brown, T. *Bioconjugate Chem.* **2006**, *17*, 1561−1567.


**10.1021/ja0715501 CCC: $37.00** **© 2007 American Chemical Society**

***Scheme 1.*** Oligomers **1**−**10** Used in This Study, Containing Phenanthrene (P) and Pyrene (S) Building Blocks or $T_6$ Loops[a]

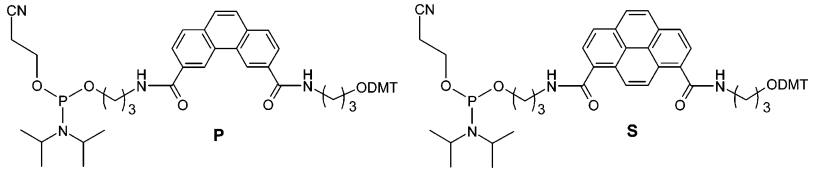


| | | |
|---|---|---|
| **1** | 5′ | AGAGAAGA TTTT TCTTCTCT **$T_6$**TCTCTTCT |
| **2** | 5′ | AGAGAAGA TTTT TCTTCTCT **P** TCTCTTCT |
| **3** | 5′ | AGAGAAGA TTTT TCTTCTCT **S** TCTCTTCT |
| **4** | 5′ **S** | AGAGAAGA TTTT TCTTCTCT **S** TCTCTTCT |
| **5** | 5′ | AGAGAAGA TTTT TCTTCTCT **P** CTTTCCTC |
| **6** | 5′ | AGAGAAGA TTTT TCTTCTCT **S** CTTTCCTC |
| **7** | 5′ | AGAGAAGA TTTT TCTTCTCT **$T_6$** CTTTCCTC |
| **8** | 5′ | GAAAGGAG TTTT CTCCTTTC **P** TCTCTTCT |
| **9** | 5′ | GAAAGGAG TTTT CTCCTTTC **S** TCTCTTCT |
| **10** | 5′ | GAAAGGAG TTTT CTCCTTTC **$T_6$** TCTCTTCT |

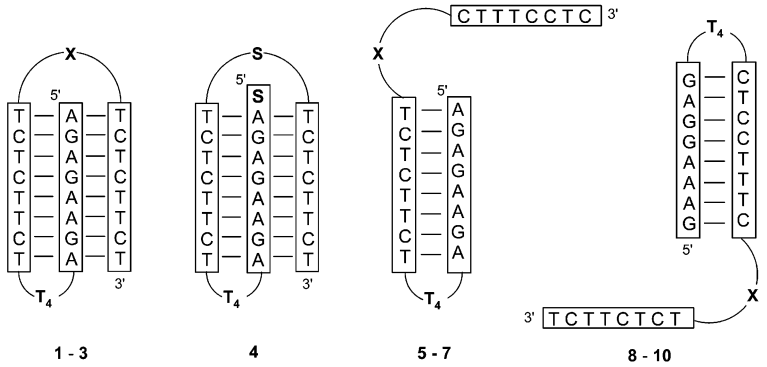


[a] The bottom part is a schematic illustration of triplex and hairpin structures formed by the respective oligomers. For simplicity, S and P are used for both, phosphoramidites as well as incorporated building blocks; DMT = 4,4′-dimethoxytrityl; X = S or P.

matic building blocks and their incorporation into DNA.[37−39] In particular, phenanthrene derivatives were shown to be excellent substitutes for the loop part of hairpin structures.[35] We have subsequently extended these studies to the investigation of potential mimics of intramolecular triple helices containing non-nucleosidic phenanthrene building blocks. In addition, we also used pyrene derivatives, which are of special interest owing to their fluorescence properties. Here, we report the synthesis of intra- and intermolecular triple helical mimics containing phenanthrene and pyrene building blocks and their remarkable structural stability.

## Results and Discussion

The synthesis of the pyrene and phenanthrene phosphoramidites **S** and **P** (Scheme 1) was performed as described.[37,38] The modified oligomers were assembled by standard automated oligonucleotide synthesis and purified by reverse phase HPLC. The correct identities of the purified oligomers were verified by electrospray ionization time-of-flight (ESI-TOF) mass spectrometry.

**Intramolecular Triple Helical Mimics.** The sequences of the different oligomers (**1**−**6**) used in the first part of this study are given in Scheme 1. The design of the triple helix follows the pyrimidine motif and was based on earlier work, in which this sequence is shown by chemical probing to adopt a triple helical structure.[16] In the pyrimidine motif, specific binding of the third strand occurs via formation of T•AT and $C^+$•GC base triplets. Thus, the oligomers are composed of a 5′-oligopurine sequence and two oligopyrimidine stretches. The anticipated folding is illustrated in Scheme 1 (bottom, left). The purine strand and the middle pyrimidine strand are linked by a $T_4$ loop (herein referred to as Watson−Crick loop) to form a Watson−Crick duplex. The 3′-terminal pyrimidine strand is connected to the duplex via the linker **X** (Hoogsteen loop). The $T_6$ Hoogsten loop was systematically varied by replacement with a phenanthrene or pyrene building block.

The effect of replacement of the nucleotide loops by phenanthrene and pyrene building blocks on the DNA triplex stability was first analyzed by thermal denaturation experiments. At neutral pH, oligomers **1**−**4** exhibit two clearly separated transitions in the melting curves (Figure 1a). The first one is characteristic for the triplex/hairpin transition and the second for the hairpin/random coil transition. Oligomer **5**, which was designed not to form a triplex by introduction of mismatches into the 3′-terminal polypyrimidine strand, exhibits only one transition.

As shown in Table 1, the introduction of phenanthrene (**2**) and pyrene (**3**) moieties into the Hoogsten loop stabilizes the triplex at neutral pH ($\Delta T_{m1}$ = 3.1 °C and 1.5 °C, respectively). The stabilizing effect is more pronounced in the second transition, since $T_{m2}$ is elevated by approximately 5 °C for both oligomers. Oligomer **4**, containing an additional pyrene moiety at the 5′-end, was designed and synthesized to further investigate

(37) Langenegger, S. M.; Häner, R. *Helv. Chim. Acta* **2002**, *85*, 3414−3421.
(38) Langenegger, S. M.; Häner, R. *Chem. Commun.* **2004**, 2792−2793.
(39) Langenegger, S. M.; Häner, R. *ChemBioChem* **2005**, *6*, 2149−2152.

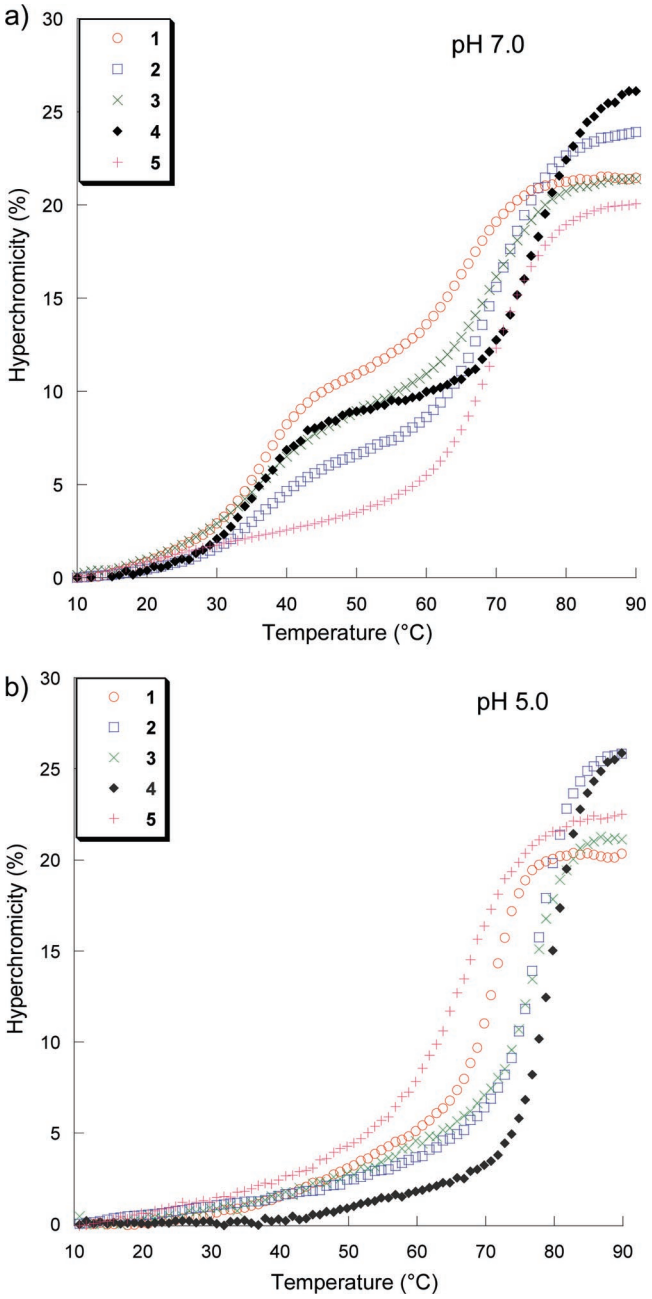


***Figure 1.*** Melting curves of different intramolecular triplexes **1**−**5**. Conditions: oligomer concentration 1.0 $\mu$M; 100 mM NaCl; 20 mM $MgCl_2$; absorbance was measured at 260 nm; (a) pH 7.0, 10 mM sodium cacodylate buffer; (b) pH 5.0, 10 mM sodium acetate buffer. Cooling curves are shown (90−10 °C).

triplex formation (see also below). A large increase of $T_{m2}$ of 11.7 °C is observed for this oligomer indicating a strong stacking interaction between the pyrene moiety at the 5′-end and the one used as Hoogsteen loop replacement. The overall increase in stability seems to be a result of stabilization of the hairpin structure rather than the triplex. As can be seen from the respective $T_{m1}$ (36.2 °C compared to 37.2 °C for oligomer **3**), the presence of the second pyrene even has a slightly negative influence on the binding of the third strand. This behavior can be rationalized by optimal stacking interactions between the two pyrenes in the hairpin structure. Upon structural reorganization due to the binding of the third strand, this interaction becomes less favorable. At pH 5.0, a single transition is observed in the

***Table 1.*** Influence of Replacement of the Hoogsten Loop with Non-nucleosidic Phenanthrene (P) and Pyrene (S) Building Blocks on Intramolecular Triplex Formation

| | | pH 7.0 | | | | pH 5.0 | |
|---|---|---|---|---|---|---|---|
| | X (Hoogsten loop) | $T_{m1}$ °C | $\Delta T_{m1}$ °C[a] | $T_{m2}$ °C | $\Delta T_{m2}$ °C[a] | $T_m$ °C | $\Delta T_m$ °C[a] |
| **1** | $T_6$ | 35.7 | | 64.8 | | 71.7 | |
| **2** | P | 38.8 | 3.1 | 70.1 | 5.3 | 79.0 | 8.3 |
| **3** | S | 37.2 | 1.5 | 69.6 | 4.8 | 78.5 | 6.8 |
| **4** | S | 36.2 | 0.5 | 76.4 | 11.7 | 81.0 | 9.3 |
| **5** | P | | | (70.1)[b] | (5.3) | (67.6)[b] | (−4.1) |
| **6** | S | | | (69.8)[b] | (5.0) | (67.3)[b] | (−4.4) |

[a] Difference in $T_m$ relative to the control **1**. [b] Tm of the hairpin structure (**5** and **6** are designed not to form a triplex).

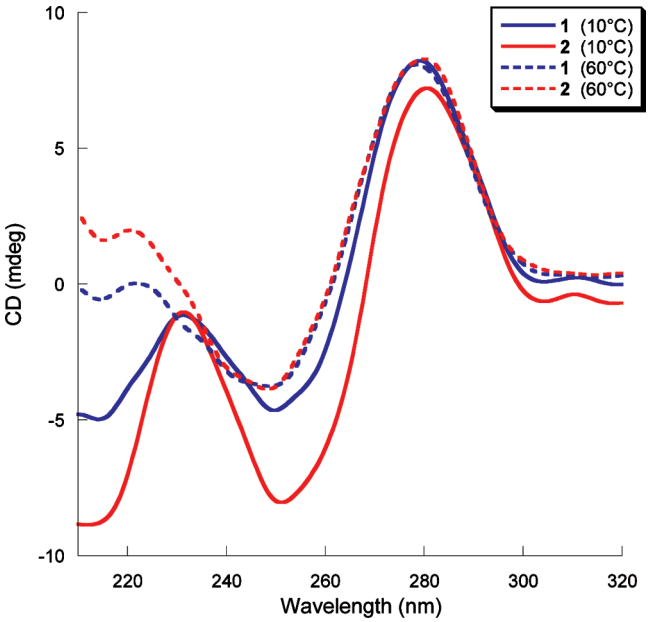


***Figure 2.*** CD Spectra of **1** and **2**. Conditions: Oligomer concentration 1.0 $\mu$M; 100 mM NaCl; 20 mM $MgCl_2$; absorbance was measured at 260 nm; pH 7.0; 10 mM sodium cacodylate buffer.

melting curves of oligomers **1**−**4**, indicative of a transition from triplex directly to random coil (Figure 1b). This is in agreement with previous findings on intramolecular triple helical structures of the pyrimidine motif.[20] Oligomers **2** and **3** form a considerably more stable structure than the unmodified triplex **1** ($\Delta T_m$ = 8.3 °C and 6.8 °C, respectively) at acidic pH. Again, oligomer **4**, which possesses two pyrene residues, exhibits the largest increase in $T_m$ (9.3 °C). Both control oligomers **5** and **6**, which can form hairpin but not triplex structures, show a slight decrease in their $T_m$ value at pH 5.0 in comparison to neutral conditions. In agreement with a monomolecular hybridization process, the $T_m$ values of oligomers **1**−**6** showed no concentration dependence within the range of 1−5 $\mu$M.

Further structural information was obtained by CD (circular dichroism) experiments. At 10 °C, well below the melting temperature of the triplex structure, the unmodified oligonucleotide **1**, as well as the phenanthrene modified oligomer **2**, exhibits a negative Cotton effect at around 214 nm and a maximum at 231 nm (Figure 2). The presence of a minimum below 230 nm was shown to be characteristic for triple helical structures.[40,41] The disappearance of this minimum at higher

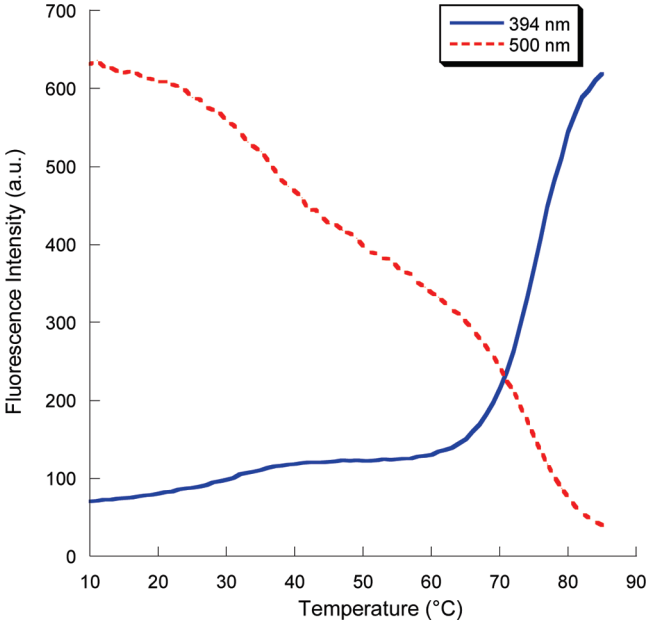


***Figure 3.*** Temperature-dependent fluorescence measurements of **4** at pH 7.0. Cooling curves are shown (85−10 °C).

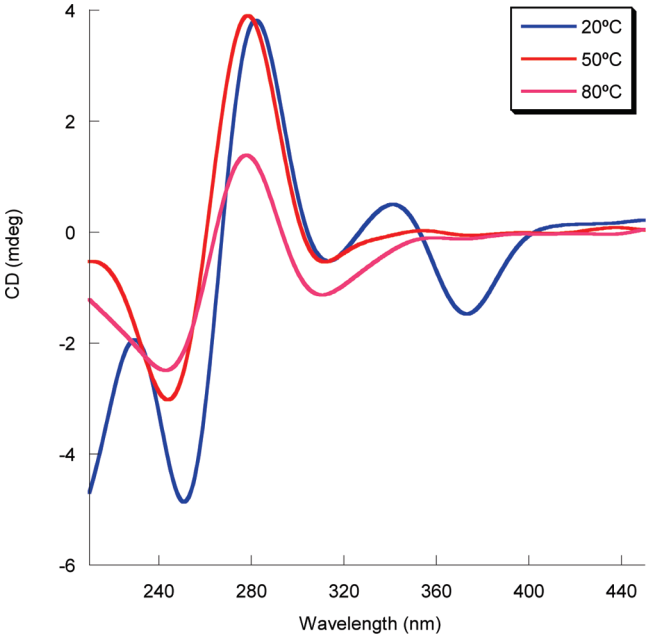


***Figure 4.*** CD spectra of triplex **4** at pH 7.0. Conditions: oligomer concentration 1.5 $\mu$M, 100 mM NaCl, 20 mM $MgCl_2$, 10 mM sodium cacodylate buffer pH 7.0.

temperature (60 °C) is indicative for the melting of the triplex to the duplex structure.[42]

Pyrene modified oligonucleotides have been used to monitor triplex formation. In particular, excimer formation can serve as a tool for structural investigation.[43−45] Therefore, oligomer **4** with an additional pyrene building block at its 5′-end (see Scheme 1) was used to further characterize the structure of the triple helical mimics. Formation of the intramolecular triplex brings the two pyrenes in close proximity. This results in excimer fluorescence which can be used to monitor the hybridization process. The thermal denaturation curve thus obtained at neutral pH is shown in Figure 3. In addition to the excimer fluorescence (500 nm) also the pyrene monomer fluorescence (394 nm) was recorded. With increasing temperature, the intensity of the excimer signal decreases showing two transitions, one at 37 °C and one at 75 °C. These values correlate well with the $T_m$ values determined by UV absorbance (36.2 and 76.4 °C, Table 1). The same effect is observed at 394 nm: monomer fluorescence is restored with increasing temperature revealing the separation of the two pyrenes as a consequence of progressing strand dissociation. The two transitions (35 °C and 76 °C) coincide with the ones observed at 500 nm. At both wavelengths, the transition at higher temperature (i.e., hairpin ⇌ random coil) is more pronounced than the one at lower temperature (triplex ⇌ hairpin). It can, thus, be concluded that the two pyrenes are also associated in the hairpin structure, albeit to a somewhat lesser extent than in the triplex structure. This finding is in agreement with a previous report describing excimer formation by pyrenes attached to the terminal positions of an oligonucleotide hairpin.[46]

Measurement of CD spectra of oligomer **4** resulted in an observation that brought further insight into the nature of the relative positioning of the two pyrenes in this structure. At 20 °C (Figure 4), a pronounced bisignate signal for the pyrene band centered at 357 nm is observed with a negative Cotton effect at $\lambda = 373$ nm ($\Delta\epsilon = -30$ $M^{-1}$ $cm^{-1}$) followed by a maximum at $\lambda = 341$ nm ($\Delta\epsilon = +10$ $M^{-1}$ $cm^{-1}$). The negative amplitude ($A = -40$) observed in the exciton coupled CD reveals a *negative chirality*, which is defined as a left handed helical arrangement of the transition dipole moments of two pyrenes.[41] Since this signal can be attributed solely to pyrene absorbance, this translates into a left-handed helical orientation of the two pyrenes. At 50 °C, the CD couplet in the pyrene 350 nm region has disappeared indicating a change in the relative orientation of the pyrenes. This is explained by the dissociation of the third strand, which takes place well below this temperature ($T_m$ = 36.2 °C, Table 1). The spectrum adopts the features of a normal B-DNA, which is expected for the remaining hairpin structure. Triplexes formed by oligomers **1**−**3** showed no bisignate signals in this range of the CD spectrum.

Figure 5 represents the model of a possible structure of triplex **4**, which was obtained by AMBER force-field minimization. It shows the relative orientation of the two pyrenes (highlighted in red and green). The 5′-terminal pyrene (red) is stacked on top of the pyrene serving as the Hoogsteen loop replacement, which itself is stacked onto the adjacent base triplet of the triplex stem. As can be seen from the calculated transition dipole moments (Figure 5, lower right), the two pyrenes are arranged in a left-handed helical orientation.

**Intermolecular, Heterodimeric Triple Helical Structures.** The sequences of oligomers **5**−**10** were designed not to form *intramolecular* but, instead, heterodimeric *intermolecular* triple helices. Each of the oligomers can, by itself, adopt a hairpin

(40) Callahan, D. E.; Trapane, T. L.; Miller, P. S.; Ts'o, P. O.; Kan, L. S. *Biochemistry* **1991**, *30*, 1650−1655.
(41) Berova, N.; Nakanishi, K.; Woody, R. W. Circular Dichroism - Principles and Applications; Wiley-VCH: New York, 2000.
(42) Mayer, A.; Häberli, A.; Leumann, C. J. *Org. Biomol. Chem.* **2005**, *3*, 1653−1658.
(43) Mohammadi, S.; SlamaSchwok, A.; Leger, G.; ElManouni, D.; Shchyolkina, A.; Leroux, Y.; Taillandier, E. *Biochemistry* **1997**, *36*, 14836−14844.
(44) Trkulja, I.; Biner, S. M.; Langenegger, S. M.; Häner, R. *ChemBioChem* **2007**, *8*, 25−27.
(45) Trkulja, I.; Häner, R. *Bioconjugate Chem.* **2007**, *18*, 289−292.
(46) Michel, J.; Bathany, K.; Schmitter, J. M.; Monti, J. P.; Moreau, S. *Tetrahedron* **2002**, *58*, 7975−7982.

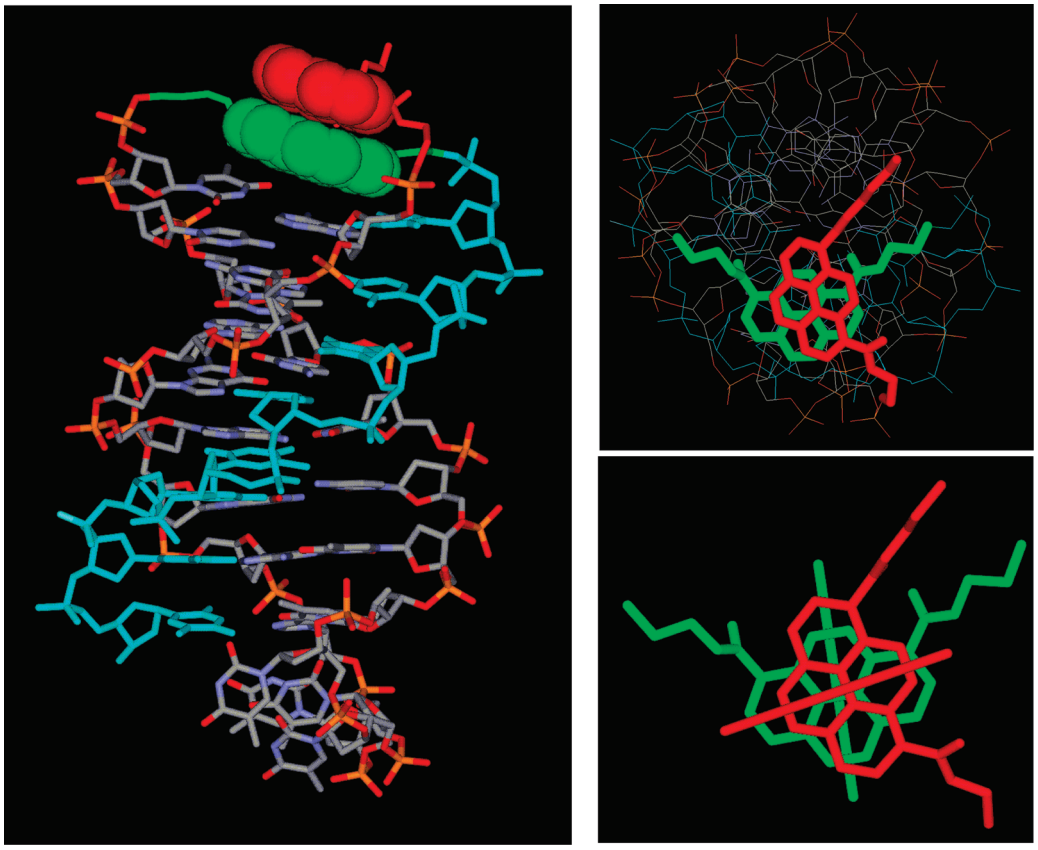

***Figure 5.*** Calculated model of triplex **4**, showing the two pyrenes (displayed in red and green) in a left-handed helical orientation. The left panel is a view perpendicular to the helical axis, pyrenes are highlighted in space filling mode. The homopyrimidine Hoogsten strand is shown in cyan. The upper-right panel is a view along the helical axis; the lower-right panel is a representation of the relative orientation of the two pyrene building blocks including the calculated transition dipole moments.

***Scheme 2.*** Schematic Representation of Formation of Intermolecular Triple Helical Hybrids between Oligomers **5**−**7** and **8**−**10**[a]

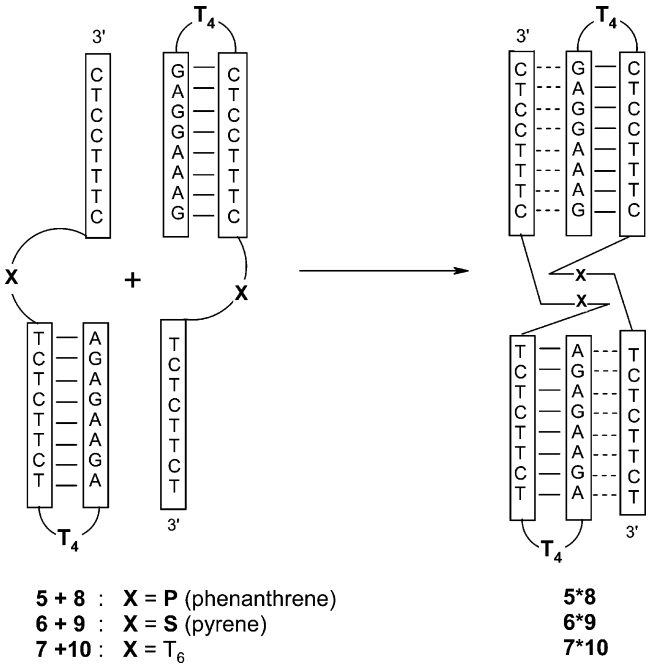


[a] Watson−Crick and Hoogsteen-type pairing are indicated by solid and dashed lines, respectively.

structure with a dangling 3′-arm attached via a phenanthrene, pyrene, or a $T_6$-sequence. Under triplex favoring conditions, however, oligomers **5**−**7** may form intermolecular structures with oligomers **8**−**10**, as illustrated in Scheme 2.

Thermal melting experiments performed at neutral and acidic pH are shown in Figures 6a and b, respectively. At neutral pH, two sharp transitions were observed for the phenanthrene and pyrene modified hybrids **5***8 and **6***9, the first one indicative of the triplex ⇌ hairpin transitions and the second one of the hairpin ⇌ random coil transitions. With both of these heterodimeric hybrids, the two triplex melting and the two hairpin melting processes cannot be observed individually. Since the two individual oligomers forming the heterodimeric structure are identical in length and very similar in base composition, the respective strand dissociations occur simultaneously resulting in only two (rather than four) observable transitions. For the unmodified heterodimeric triplex (**7***10), only the hairpin ⇌ random coil transition could be observed ($T_m$ = 66.8 °C). Thus, in comparison to the hybrid with $T_6$ linkers, the phenanthrene as well as the pyrene modification results in a considerable stabilization of the triple helical structures. In both cases, an increase of the $T_{m1}$ of more than 10 °C (Table 2) was noted. Furthermore, a high increase was also observed for $T_{m2}$ in both of the modified hybrids at neutral pH, in accordance to the findings stated above that the aromatic moieties stabilize not only the triplex but also the hairpin structure. At acidic pH, all three hybrids show a single transition in the denaturation curves revealing a direct triplex ⇌ random coil transition. The $T_m$ values (Table 2) are increased by 14.9 and 13.2 °C for the

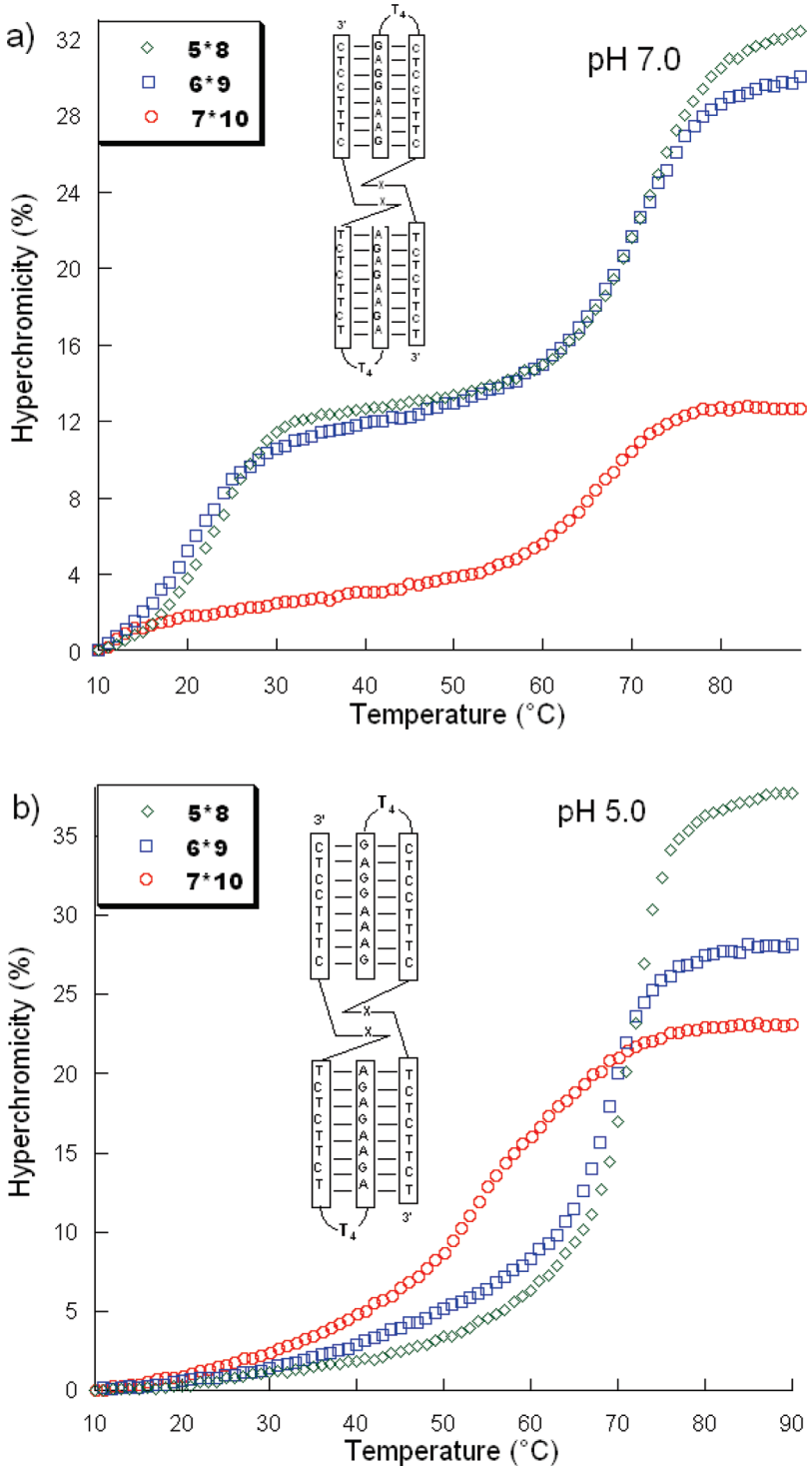


***Figure 6.*** Melting curves of different intermolecular triplexes. Conditions: oligomer concentration 1.5 $\mu$M, 100 mM NaCl, 20 mM $MgCl_2$; (a) pH 7.0, 10 mM sodium cacodylate buffer; (b) pH 5.0, 10 mM sodium acetate buffer. Cooling curves are shown (90−10 °C).

phenanthrene (**5*8**) and pyrene (**6*9**) containing hybrids, respectively.

Fluorescence spectroscopy was used to further investigate possible interactions between the pyrene building blocks in the heterodimer **6*9** (Figure 7). Upon excitation at 356 nm, oligomer **6** exhibits pyrene monomer fluorescence only ($\lambda_{max}$ = 394 nm). The heterodimer **6*9**, on the other hand, clearly shows a second band at 500 nm, which is characteristic of pyrene excimer formation. Although the excimer signal is weaker than the monomer fluorescence, this indicates proximity of the two pyrenes and provides solid evidence for the dimeric structure illustrated in Scheme 2. The dimerization of complementary oligomers **6** and **9** brings the two pyrenes together enabling excimer formation between them. The monomer-to-excimer ratio of 3:1 in the fluorescence studies of this hybrid further indicates that, while the pyrenes are close enough to form an excimer, they are not aggregated previous to excitation, thus exhibiting an excimer signal of lower intensity.[47] Furthermore, fluorescence

(47) Winnik, F. M. *Chem. Rev.* **1993**, *93*, 587−614.

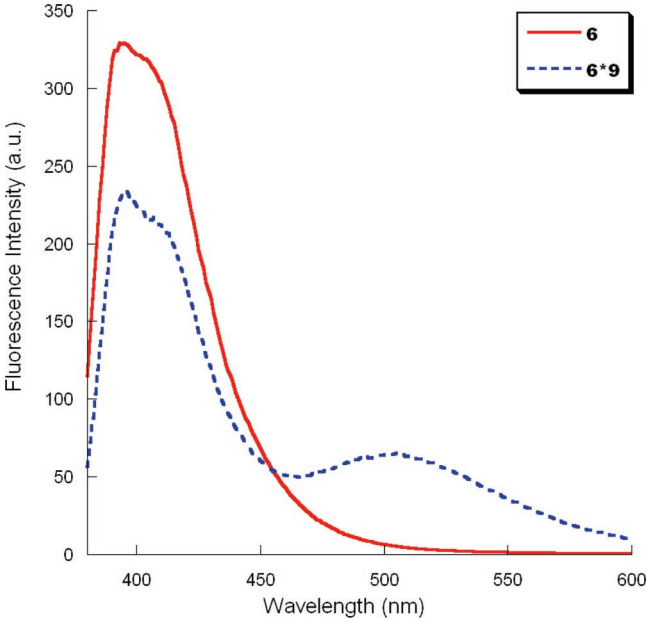


***Figure 7.*** Fluorescence spectra for oligomer **6** and hybrid **6*9**. Conditions: oligomer concentration 1.5 $\mu$M, 100 mM NaCl, 20 mM $MgCl_2$; pH 5.0; 10 mM sodium acetate buffer. Excitation wavelength, 356 nm; excitation slit, 10 nm; emission slit, 5 nm.

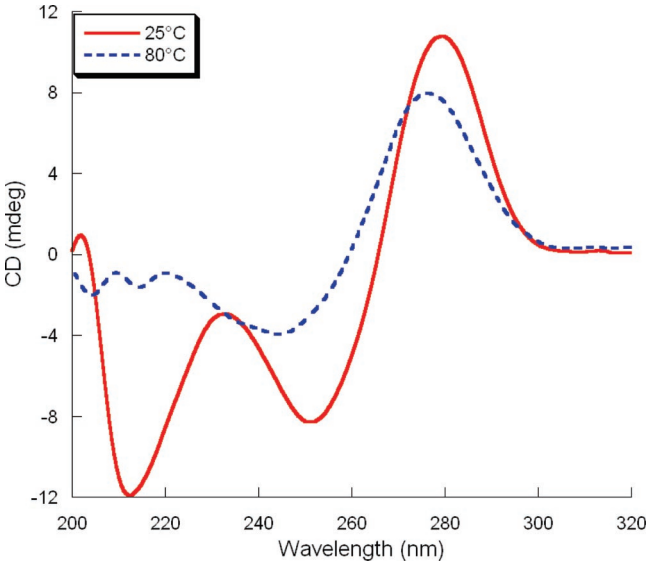


***Figure 8.*** CD Spectra of pyrene-modified intermolecular triplex **6*9**. Conditions: oligomer concentration 1.5 $\mu$M, 100 mM NaCl, 20 mM $MgCl_2$; pH 5.0; 10 mM sodium acetate buffer.

***Table 2.*** $T_m$ Values of Different Heterodimers

| | X (Hoogsten loop) | pH 7.0 $T_{m1}$ °C | pH 7.0 $\Delta T_{m1}$ °C[a] | pH 7.0 $T_{m2}$ °C | pH 5.0 $T_m$ °C | pH 5.0 $\Delta T_m$ °C[a] |
|---|---|---|---|---|---|---|
| **5*8** | P:P | 22.0 | >12 | 72.1 | 71.2 | 14.9 |
| **6*9** | S:S | 20.1 | >10 | 70.5 | 69.5 | 13.2 |
| **7*10** | $T_6$:$T_6$ | <10 | | 66.8 | 56.3 | |

[a] Difference in $T_m$ relative to unmodified hybrid **7*10**

measurements with oligomer **6** at higher concentrations (up to 3.5 $\mu$M) revealed no excimer signal, which excludes excimer formation due to self-aggregation (data not shown).

***Table 3.*** Summary of Mass Spectrometry Data for Oligonucleotides Synthesized in This Study[a]

| oligonucleotide | calculated MW-1 | found |
|---|---|---|
| **1** | 10309.8 | 10308.8 |
| **2** | 8925.7 | 8925.6 |
| **3** | 8950.6 | 8949.1 |
| **4** | 9416.6 | 9416.2 |
| **5** | 8911.6 | 8910.8 |
| **6** | 8935.6 | 8935.3 |
| **8** | 8927.6 | 8925.7 |
| **9** | 8951.6 | 8950.3 |

[a] Unmodified oligonucleotides **7** and **10** were obtained from Microsynth AG, Switzerland

Finally, intermolecular triplex formation was confirmed for hybrid **6*9** by CD measurement at acidic pH (Figure 8). At 25 °C, that is, below the triplex melting temperature, a maximum at 233 nm and a minimum at 212 nm is observed, which is in agreement with a triple helical structure.[40,41] At higher temperature (80 °C), the triplex-characteristic features have disappeared.

## Conclusions

The data presented in this work demonstrate that intra- and intermolecular triple helices of the pyrimidine motif can be stabilized by replacement of the natural nucleotides in the *Hoogsteen* loop with pyrene and phenanthrene building blocks. The increase in the stability of the triple helical structures can be attributed to favorable stacking interactions of the polyaromatic moieties with the adjacent bases of the triple helical stem. The appearance of an exciton coupled CD signal in the pyrene absorbance demonstrates a tight interaction between two pyrenes as a result of intramolecular triple helix formation. The shape of the bisignate signal reveals that the two pyrenes are stacked to each other in a left-handed orientation. Furthermore, the construction of *heterodimeric triple helical architectures* is described. As in the case with intramolecular structures, these intermolecular hybrids are considerably stabilized ($\Delta T_m$ up to 15 °C) by pyrene and phenanthrene derivatives. Dimer formation by two oligomers is aided by interactions between the polyaromatic building blocks as monitored by excimer formation between the pyrenes of the two individual oligomers. These findings are important for the design and construction of nucleic acid based triple helical architectures and, thus, help in the development of artificial triplex structures[48] with biomimetic functions.[49]

## Experimental Section

**General.** Reagents used for synthesis of pyrene and phenanthrene phosphoramidites were purchased from Fluka, Sigma-Aldrich or Acros and were used without further purification.

**Preparation of DNA Oligomers. Preparation of the Oligonucleotides.** Oligonucleotides were synthesized on a 392 DNA/RNA Synthesizer (Applied Biosystems) according to standard phosphoramidite chemistry. The nucleoside phosphoramidites were from Transgenomic (Glasgow, U.K.). The standard synthetic procedure ("trityl-off" mode) was used to synthesize the oligonucleotides. Detachment from the solid support and final deprotection was achieved by treatment with 30% ammonium hydroxide for 14 h at 55 °C. The crude

(48) Mateos-Timoneda, M. A.; Kerckhoffs, J. M. C. A.; Reinhoudt, D. N.; Crego-Calama, M. *Org. Biomol. Chem.* **2007**, *5*, 447−449.
(49) Fiammengo, R.; Crego-Calama, M.; Reinhoudt, D. N. *Curr. Opin. Chem. Biol.* **2001**, *5*, 660−673.

oligonucleotides were purified by reverse-phase HPLC (LiChrospher 100 RP-18, 5 $\mu$m, Merck; Bio-Tek Instruments Autosampler 560); eluent A = $(Et_3NH)OAc$ (0.1 M, pH 7.4); eluent B = MeCN; elution at 40 °C; detection at 260, 280, and 310 nm. The mass spectrometry data for the purified oligonucleotides were determined by electrospray mass spectrometry: VG Platform single quadrupole ESI-MS (see Table 3). Concentrations of oligonucleotides were determined via Varian Cary-100 Bio-UV/vis spectrophotometer. For the incorporated building blocks P and S, $\epsilon_{260}$ values of 49300 and 8600, respectively, were taken as published previously.[35,38]

**Thermal Denaturation Experiments.** The experiments were carried out under the following conditions: oligonucleotide concentration 1.0 $\mu$M for intrastrand oligonucleotides and 1.5 $\mu$M of each strand for interstrand triplex hybrid experiments; 10 mM buffer (sodium cacodylate buffer for pH 7.0 and sodium acetate buffer for pH 5.0); 100 mM NaCl; 20 mM $MgCl_2$. A Varian Cary 3e UV/vis spectrophotometer equipped with a Peltier block temperature-controller and Varian WinUV software were used to determine the melting curves at 260 nm. A heating−cooling−heating cycle in the temperature range of 0−90 or 10−90 °C was applied with a temperature gradient of 0.5 °C $min^{-1}$ for experiments at pH = 5.0 and 0.2 °C $min^{-1}$ at pH 7.0. To avoid $H_2O$ condensation on the UV cells at temperatures below 20 °C, the cell compartment was flushed with $N_2$. All ramps were indicating equilibrium melting process. The data were collected and analyzed with Kaleidagraph software from Synergy Software. $T_m$ values were determined as the maximum of the first derivative of the melting curve. Each $T_m$ shown is the average of the second (cooling) and third (heating) curve of three independent experiments; experimental error was ± 0.5 °C.

**Circular Dichroism Spectra.** CD-spectra were recorded on a Jasco J-715 spectropolarimeter equipped with a Jasco PFO-350S temperature controller. The temperature was measured directly in the sample. In the case of intramolecular triplexes the strand concentration was 1.0 $\mu$M in 10 mM sodium cacodylate buffer, 100 mM NaCl, 20 mM $MgCl_2$ at pH 7.0. In the case of intermolecular triplex hybrids, the concentration of both strands was 1.5 $\mu$M in 10 mM sodium acetate buffer, 100 mM NaCl, 20 mM $MgCl_2$ at pH 5.0. The samples were scanned at a speed of 50 nm $min^{-1}$, bandwidth of 1 nm, response of 1 s and in a 210-450 nm range at constant temperature. Each spectrum was taken as an average of three scans using a 10 mm cell. Subsequently, the graphs were smoothed with a noise filter.

**Fluorescence Experiments.** Temperature-dependent fluorescence data were collected on a Varian Cary Eclipse fluorescence spectrophotometer equipped with a Varian Cary block temperature controller (excitation at 356 nm, excitation−emission slit width was 10 and 5, respectively). Conditions were analogous to CD and thermal denaturation experiments. The Varian Eclipse software was utilized to investigate the fluorescence properties of different pyrene-containing oligonucleotides at a wavelength range of 380−600 nm.

**Molecular Modeling.** The model of triplex **4** (Figure 5) was generated using Hyperchem 7.5 (Hypercube, Waterloo, Ontario). Geometry optimizations were carried out using the AMBER force field. The reported structure of an intramolecular triplex[32] served as the basis. Pyrene building blocks were inserted followed by minimization of the local structure. Transition dipole moments were calculated for pyrene-1,8-dicarboxylic acid bis-ethylamide using the same program.

**Acknowledgment.** Financial support by the Swiss National Foundation (Grant 200020-109482) is gratefully acknowledged.

JA0715501